# Enhancing Catalytic Activity of $MoS_2$ Basal Plane S-Vacancy by Co Cluster Addition

Sangwook Park,[†,▽] Joonsuk Park,[‡,▽] Hadi Abroshan,[§,▽] Liang Zhang,[∥] Jung Kyu Kim,[⊥] Jiaming Zhang,[#] Jinghua Guo,[∥] Samira Siahrostami,[*,§] and Xiaolin Zheng[*,†]

[†]Department of Mechanical Engineering, Stanford University, 440 Escondido Mall, Stanford, California 94305, United States

[‡]Department of Material Science & Engineering, Stanford University, 440 Escondido Mall, Stanford, California 94305, United States

[§]SUNCAT Center for Interface Science and Catalysis, Department of Chemical Engineering, Stanford University, 443 Via Ortega, Stanford, California 94305, United States

[∥]Advanced Light Source, Lawrence Berkeley National Laboratory, Berkeley, California 94720, United States

[⊥]School of Chemical Engineering, Sungkyunkwan University, Suwon, 16419, Republic of Korea

[#]Hewlett-Packard Laboratories, 1501 Page Mill Road, Palo Alto, California 94304, United States

**ABSTRACT: The basal plane of molybdenum disulfide ($MoS_2$) was recently activated for hydrogen evolution reaction (HER) by creating sulfur (S) vacancies ($MoS_{2-x}$). However, the HER activity of those S-vacancies depends on the concentration of S-vacancies, imposing a dilemma for either improving activity per site or increasing overall active site density. Herein, we use density functional theory (DFT) calculations and experiments to show that the HER activities of $MoS_{2-x}$ are greatly enhanced by adding cobalt (Co) clusters on the basal plane. Our DFT results show that the highest HER activity is achieved when the Co clusters are anchored on the S-vacancies with the interface of Co−Mo as the preferred active site. Our experiments confirm that the addition of Co enhances the activity per unit active site and increases the electrochemical active surface area. These results demonstrate the basal plane activity of $MoS_{2-x}$ can be enhanced by decorating S-vacancies with transition-metal clusters.**

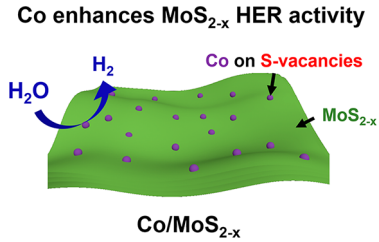


Developing efficient electrocatalysts for hydrogen evolution reaction (HER) has been widely pursued because of its importance in electrolysis to produce hydrogen ($H_2$).[1] Molybdenum disulfide ($MoS_2$) has risen up as a promising alternative to the state-of-the-art electrocatalyst Pt because of its abundance and great activity, selectivity, and stability for HER.[2−6] Previously, only the edge sites of $MoS_2$ were active for HER,[2,7,8] with a hydrogen adsorption free energy ($\Delta G_H$) of about 0.06 eV,[9] and extensive research has been dedicated to maximizing the exposed edge site density.[8,10−12] Recently, the basal plane of $MoS_2$ and molybdenum diselenide ($MoSe_2$) was successfully activated for HER by generating sulfur (S) and selenium (Se) vacancies, respectively.[3,6,13−18] Especially, S-vacancies generated by diverse methods, such as argon plasma treatment,[13] hydrogen annealing,[15] and electrochemical desulfurization,[16] were all shown to be active toward HER, demonstrating the great promise of using the basal plane of $MoS_2$ for HER.

Nevertheless, the calculated $\Delta G_H$ value for the S-vacancy over monolayer 2H phase $MoS_2$ changes from 0.2 eV to −0.2 eV when the S-vacancy concentration increases from 3% to 25% (%S-vacancy is defined as the number of S-vacancies over the total number of possible S atoms).[13] This result implies critical limitations in using the basal plane of $MoS_2$, especially multilayer $MoS_2$, for HER. First, the basal plane S-vacancy concentration needs to be precisely controlled to achieve its optimal $\Delta G_H$. Such precise control of S-vacancy concentration is challenging to realize for multilayer $MoS_2$ experimentally. Second, the optimal concentration of S-vacancy is not established for multilayer $MoS_2$, and its dependence on the number of layers is unclear. The interlayer distance of the $MoS_2$ is >3.5 Å, implying the catalytic activity of low-concentration S-vacancy at the surface of $MoS_2$ is likely independent of interlayer interactions. However, as the S-vacancy concentration increases, it becomes prudent to consider structural deformation of the top layer along with interlayer S-vacancy diffusion (Figure S1). Because of the complexity of the given system and high computational cost of working with big supercells of $MoS_2$, a comprehensive picture of the interlayer interactions and the dependence of the catalytic activity on the S-vacancy concentration for multilayer $MoS_2$ remains elusive. Third, the existence of the optimal S-vacancy concentration imposes an upper limit for the active

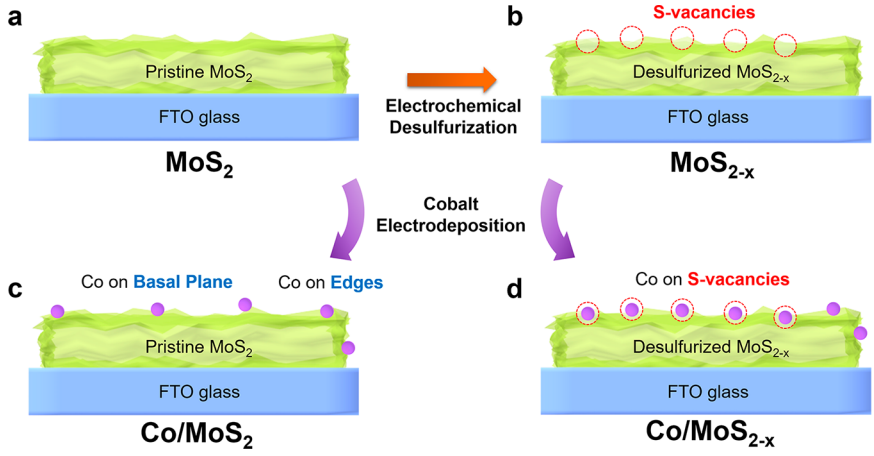


**Figure 1. Schematic of the synthesis procedures. The overall synthesis steps of Co/$MoS_{2-x}$ ($MoS_2$ with basal plane S-vacancy) and its control sample of Co/$MoS_2$ (pristine $MoS_2$) are schematically illustrated. (a) Pristine $MoS_2$ multilayers are grown on a supporting substrate (e.g., FTO glass). (b) S-vacancies are generated by electrochemical desulfurization, leading to desulfurized $MoS_{2-x}$. Finally, Co is electrodeposited on top of $MoS_2$ and $MoS_{2-x}$ to form Co/$MoS_2$ (c) and Co/$MoS_{2-x}$ (d), respectively. The detailed synthesis steps are described in the Supporting Information.**

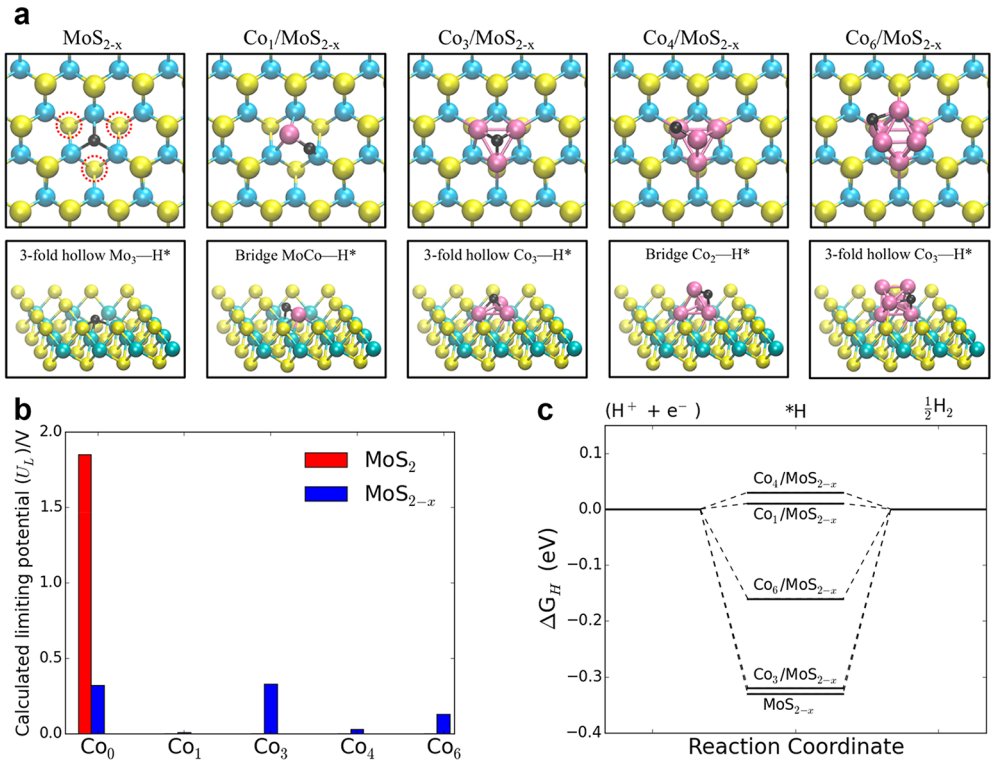


**Figure 2. DFT-calculated HER activity over $Co_n/MoS_{2-x}$. (a) Top and side views for the optimized hydrogen adsorption on desulfurized $MoS_{2-x}$ in the absence and presence of Co clusters. Three S-vacancies are marked with dashed red circles in $MoS_{2-x}$. Color code: Mo, cyan; Co, purple; S, yellow; H, black. (b) Calculated limiting potential for $MoS_{2-x}$ in the absence ($Co_0$) and presence of cobalt clusters ($Co_1$, $Co_3$, $Co_4$, and $Co_6$). (c) Free-energy diagram for $Co_n$ clusters embedded in $MoS_{2-x}$.**

site density on the basal plane of $MoS_2$. It is therefore of great interest to weaken the interdependence between the $\Delta G_H$ value of the individual S-vacancy and the concentration of S-vacancy. In practice, for a given concentration of the basal plane S-vacancy for $MoS_2$, we need to identify new ways to improve its activity for HER to fully utilize the potential of basal planes of $MoS_2$.

Cobalt (Co), as a nonprecious metal, is known to promote catalytic activity of the edge sites of $MoS_2$. In the presence of Co atoms, $MoS_2$ exhibits enhanced activity for not only HER[19−21] but also water gas shift[22,23] and oxygen reduction reactions.[24] Recently, single-site atomic Co was successfully doped in the basal plane S-vacancies of $MoS_2$, leading to a significant improvement in catalytic activity for the hydrodeoxygenation (HDO) reaction.[25]

Herein, by combining theory and experiment, we demonstrate that adding Co atoms over the basal plane of desulfurized $MoS_{2-x}$ (Figure 1) substantially enhances the HER activity. According to our DFT calculations, the Co atoms directly connected to the $MoS_{2-x}$ basal plane are the

preferred adsorption sites for hydrogen. The significant enhancement is observed when Co atoms are anchored in the S-vacancies with the interface of Co−Mo as the preferred active site, which is further supported by the XAS experiments. For Co/$MoS_2$ studied as a control sample (Figure 1c), the Co addition, mainly occurring at edge sites, does not change the electrochemical active surface area (ECSA) but enhances the activity per unit site. In contrast, for Co/$MoS_{2-x}$ (Figure 1d), the Co addition increases both the activity per active site and ECSA. For the desulfurized $MoS_{2-x}$ multilayers supported on carbon foams, the deposition of Co reduces the overpotential at −10 mA/cm$^2$ from −0.32 to −0.21 V vs RHE for Co/$MoS_{2-x}$, which is comparable to the state-of-the-art $MoS_2$-based catalysts (−0.25 to −0.11 V vs RHE).[4] These results demonstrate the effectiveness and potential of modifying the intrinsic basal plane S-vacancy activity with transition metals, which could be applied to other catalytic reactions.

*Theoretical Analysis*. According to previously reported DFT analysis, single S-vacancies in $MoS_2$ significantly promote the HER activity.[16] However, the separated small S-vacancies are not thermodynamically stable and tend to agglomerate and form larger S-vacancies. A too high concentration of S-vacancies leads to a too strong interaction of HER intermediate (H*) with the $MoS_2$ basal plane, lowering the HER activity as reported previously.[16]

Our strategy to maintain the high HER activity of the S-vacancies in the basal plane is to embed Co clusters in the S-vacancies. We calculate the hydrogen adsorption free energy ($\Delta G^0_{H^*}$) over a monolayer series of desulfurized $MoS_{2-x}$ (Figure 2a) with different Co clusters ($Co_n$ with $n$ = 0, 1, 3, 4, and 6) and find the limiting potential ($U_L = |\Delta G^0_{H^*}|/e$) (see Computational Details in the Supporting Information) to estimate the activity. The equilibrium potential for HER is 0.0 V, and a lower calculated $U_L$ represents a higher activity.

Figure 2b compares the $U_L$ for the various structures in Figure 2a, and Figure 2c displays the free energy diagram for HER over $MoS_{2-x}$ in the presence and absence of embedded $Co_n$ clusters. According to our DFT calculations, the pristine $MoS_2$ binds H* very weakly, resulting in a $U_L$ of ∼ 1.90 V, in agreement with the previous report.[16] Removal of a single S atom from the pristine $MoS_2$ (S-vacancy percentage ≈ 3.1%) strengthens the interaction of H* with the remaining framework with $U_L$ ≈ 0.10 V, indicating a considerable improvement in HER activity. It is worth noting that the single S-vacancies thermodynamically favor aggregating to form larger S-vacancies that tend to adsorb H* strongly and hence poison the catalyst. For example, removal of three sulfur atoms from the $MoS_2$ slab results in a triangle-shaped vacancy (Figure 2a, left; S-vacancy percentage ≈ 9.4%). Such a vacancy exposes three Mo atoms, which favorably adsorb H* leading to $U_L$ ≈ 0.33 V (Figure 2b, $Co_0$, blue bar). Expanding the triangle-shaped S-vacancy by removal of the next three nearest sulfur atoms (Figure S2, S-vacancy percentage ≈ 18.8%) results in a stronger hydrogen adsorption free energy with $U_L$ ≈ 0.54 V. We next consider the presence of Co atoms on the HER activity of the $MoS_2$.

A previous study by Liu et al. showed that the addition of Co complexes to a solution of $MoS_2$ leads to the accommodation of single Co atoms on the basal plane of $MoS_2$.[25] A single Co atom can chemisorb on one of the two chemically nonequivalent $S_3$ sites at the surface of $MoS_2$, namely hollow and Mo atop sites (Figure S3A and S3B). These single Co atoms prefer to migrate and fill a nearby single S-vacancy that may form because of elevated temperature (S atop site, Figure S3C).[25] Of note, the later configuration is equivalent to one generated by substitution of a sulfur atom with a single Co. Our DFT results show a chemisorbed Co atom on the hollow, Mo atop, or S atop sites adsorbs H* with $\Delta G^0_{H^*}$ = 0.67, 0.40, and 0.64 eV, respectively. This indicates that these sites would present considerable overpotentials for HER. We next investigate HER activity of an embedded Co on a larger S-vacancy.

The substitution of a sulfur atom by Co can promote the generation of proximal S-vacancy in an exothermic manner.[25] Therefore, we consider removal of two sulfur atoms in the vicinity of an embedded Co and evaluate HER activity. Of note, there are two possible configurations for the removal of two sulfur atoms near the Co, i.e., $Co_1/MoS_{2-x(a)}$ and $Co_1/MoS_{2-x(b)}$, Figure S4. These configurations adsorb H* favorably with $U_L$ ≈ 0.25 and 0.13 V, respectively. It is worth noting that the embedded Co atom may migrate to bond with three Mo atoms around the hollow site with $U_L$ ≈ 0.01 V ($Co_1/MoS_{2-x(c)}$, Figure S4). The calculated formation energies are almost similar (within ∼0.1 eV) for all these three configurations of $Co_1/MoS_{2-x}$. The H* is preferentially adsorbed at the interface of Co−Mo for $Co_1/MoS_{2-x(a)}$ (Figure S5) and $Co_1/MoS_{2-x(c)}$ (Figure 2a, second left), while for $Co_1/MoS_{2-x(b)}$ the cavity composed of three Mo and the Co is the active site (Figure S5). In addition to single Co atoms, we also examined the activity of other $Co_n$ clusters ($n$ = 3, 4, 6) embedded in the vacancies of $MoS_{2-x}$. For $Co_n/MoS_{2-x}$ systems, several configurations are examined via DFT optimization, and the most stable ones are reported here. As shown in Figure 2b, the calculated $U_L$ values over $Co_3/MoS_{2-x}$, $Co_4/MoS_{2-x}$, and $Co_6/MoS_{2-x}$ structures are 0.33, 0.03, and 0.13 V, respectively, which are lower than that of $MoS_{2-x}$ and $MoS_2$. Therefore, the HER activity decreases in the order of $Co_n/MoS_{2-x}$ > $MoS_{2-x}$ > $MoS_2$. The preferred adsorption site for H* over $Co_3/MoS_{2-x}$ and $Co_6/MoS_{2-x}$ is the 3-fold hollow site (Figure 2a). Among several possible 3-fold hollow sites in the supported $Co_6$, those with cobalt atoms directly connected to the supports are favored. For the $Co_4/MoS_{2-x}$, the Co−Co bridge site is the preferred active site, where one of the Co atoms involved in the adsorption is directly connected to the $MoS_2$ substrate (Figure 2a).

The theoretical results presented above reveal desirable synergic effects between additional Co atoms and $MoS_2$ support and offer a potentially interesting system for achieving significantly high HER activity. The most salient aspect of our DFT results is that the HER activity can be drastically improved in the presence of embedded Co atoms in the S-vacancies with the interface of Co−Mo being the most active motif. While our DFT study reported here contributes novel insights on the promotional effect of Co atoms on HER activity of $MoS_2$, some aspects are not properly accounted for in our analysis because of high computational expenses. These include the influence of Co clusters and S-vacancy size on the HER activity. Therefore, it would be worthwhile in the future to extend the current DFT study to bigger metal clusters embedded on a wide range of S-vacancies and their effect on HER catalytic activity.

*Synthesis of Co/$MoS_2$ and Co/$MoS_{2-x}$*. To support our theoretical results, we experimentally investigate the HER activity of the basal plane S-vacancy for $MoS_2$ (i.e., desulfurized $MoS_{2-x}$) multilayers in the presence of electrodeposited Co atoms. We synthesized polycrystalline 2H phase $MoS_2$

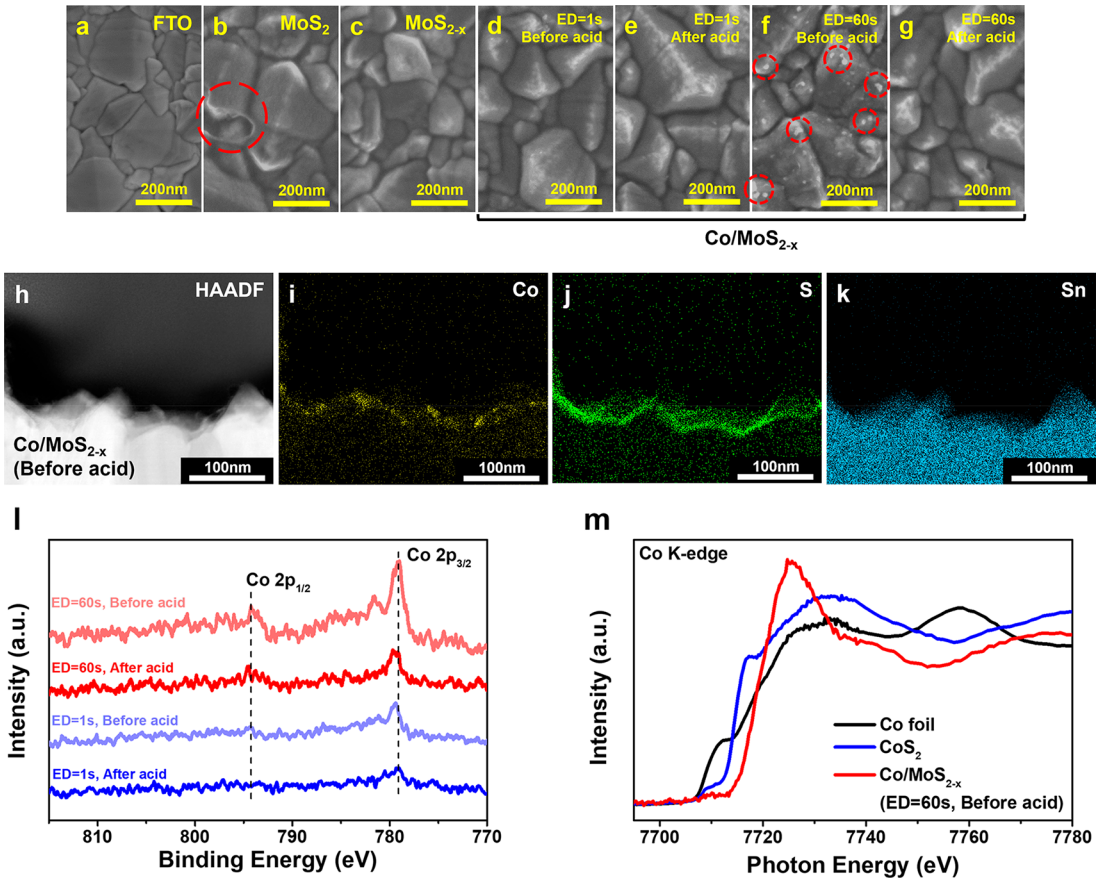


**Figure 3. Materials characterization of $Co/MoS_{2-x}$ film on FTO substrate. (a–g) SEM images of FTO, $MoS_2$, $MoS_{2-x}$, $Co/MoS_{2-x}$ (ED = 1 s, before and after acid etching), and $Co/MoS_{2-x}$ (ED = 60 s, before and after acid etching). ED refers to electrodeposition time of Co. (h–k) STEM image of $Co/MoS_{2-x}$ (ED = 60 s, before acid etching) (h) and corresponding EDS elemental mappings of Co, S, and Sn, respectively (i–k). (l) XPS spectrum of Co 2p region of $Co/MoS_{2-x}$ (ED = 1 s and 60 s) before and after acid etching. (m) Co K-edge XANES spectra of Co metal foil, $CoS_2$ and $Co/MoS_{2-x}$ (ED = 60 s, before acid etching).**

multilayers supported on FTO glasses (Figure 1a) or carbon foams through thermolysis.[26] S-vacancies were generated on the basal plane of $MoS_2$ using the electrochemical desulfurization method that we developed previously[16] (Figure 1b). Co was electrodeposited onto both pristine $MoS_2$ ($Co/MoS_2$) and desulfurized $MoS_{2-x}$ ($Co/MoS_{2-x}$) for comparison purposes. Because the basal plane S-vacancy is coordinatively unsaturated like edge sites, the deposited Co atoms are expected to be incorporated mainly at the edge sites for $Co/MoS_2$ (Figure 1c) but on both the basal planes and the edge sites for $Co/MoS_{2-x}$ (Figure 1d).

*Morphology and Composition Characterization of $Co/MoS_{2-x}$ on FTO*. Panels a–g of Figure 3 show the scanning electron microscopy (SEM) images of bare FTO, pristine $MoS_2$, desulfurized $MoS_{2-x}$, $Co/MoS_{2-x}$ (ED = 1 s, before and after acid etching), and $Co/MoS_{2-x}$ (ED = 60 s, before and after acid etching). After synthesis of pristine $MoS_2$, the transparent FTO becomes dark brownish. Although the grain of FTO remains clear, small holes in $MoS_2$ can be observed in Figure 3b (red dotted circle). The composition of 2H phase $MoS_2$ multilayers is further confirmed by both Raman spectra (Figure S6a) and X-ray photoelectron spectroscopy (XPS) measurement (Figure S6b,c). After desulfurization, no significant morphology or color change can be observed between pristine $MoS_2$ (Figure 3b) and desulfurized $MoS_{2-x}$ (Figure 3c). After 1 s of ED Co, the SEM image does not show any visible morphology change (Figure 3d) and the XPS spectrum shows a small Co $2p_{3/2}$ peak at 779.1 eV (Figure 3l). Other than XPS, it is difficult to characterize the existence of Co because of its small amount. To further confirm the deposition of Co, we also inspected the $Co/MoS_{2-x}$ sample with a much longer ED time of 60 s, which clearly shows the small particle formation on top (Figure 3f, red dotted circles). In addition, the $Co/MoS_{2-x}$ (ED = 60 s) clearly shows two main Co 2p peaks of Co $2p_{3/2}$ at 779.1 eV and another Co $2p_{1/2}$ at 794.5 eV (Figure 3l). The cross-sectional scanning transmission electron microscopy-high-angle annular dark field (STEM-HAADF) image of $Co/MoS_{2-x}$ (ED = 60 s) shows that the thickness of $MoS_2$ multilayer is around 10 nm (Figure 3h). The thickness is also confirmed by the EDS elemental maps of S and Sn element (Figure 3j,k). The Co mapping from the above Co–K peak (~6.9 keV) shows that Co exists in small particles with size from a few nanometers to ~10 nm in the $Co/MoS_{2-x}$ (ED = 60 s) sample (Figure 3i). Similar elemental distributions are observed by TEM and STEM-HAADF images and EDS elemental mappings of other areas (Figures S7 and S8). HRTEM images show that the Co particles (ED = 60 s) are CoO nanoparticles (Figure S9).

Those characterizations confirm the deposition of Co onto $MoS_{2-x}$. However, our HER measurement is carried out in strong acidic conditions, where CoO is not stable. To test if some Co will remain during the HER, we soaked $Co/MoS_{2-x}$ of both ED = 1 s and ED = 60 s in 0.5 M $H_2SO_4$ for around 1 min and compared the SEM and XPS afterward. For the Co/

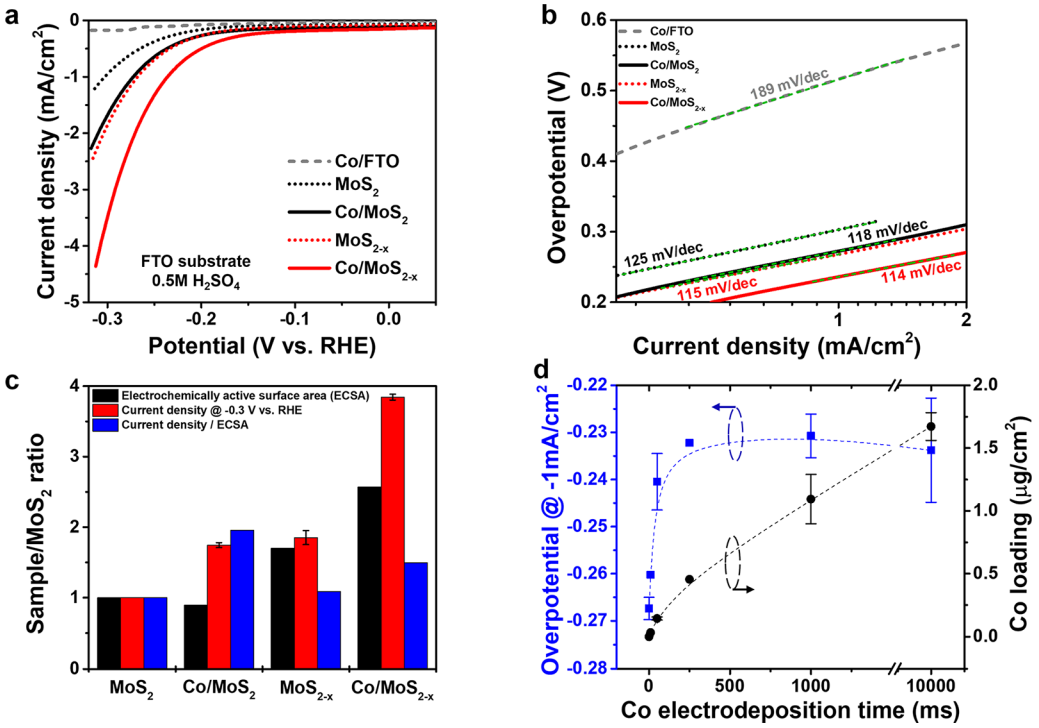


**Figure 4. HER catalytic activity of Co, $MoS_2$, $MoS_{2-x}$, $Co/MoS_2$ (ED = 1 s), and $Co/MoS_{2-x}$ (ED = 1 s) supported on FTO substrate. (a) Polarization curves. (b) Tafel plots of the cathodic sweeps of the polarization curves in panel a. (c) Normalized electrochemically active surface area (black), current density ratio at −0.3 V vs RHE (red), and current density/ECSA (blue) for $MoS_2$, $MoS_{2-x}$, $Co/MoS_2$ (ED = 1 s), and $Co/MoS_{2-x}$ (ED = 1 s) over those of $MoS_2$. (d) Overpotential of $Co/MoS_{2-x}$ at −1 mA/cm² (left axis) and the corresponding Co loading (right axis) as a function of Co electrodeposition time.**

$MoS_{2-x}$ (ED = 1 s) sample, both the SEM image (Figure 3e) and XPS spectrum (Figure 3l) show little difference, and the Co $2p_{3/2}$ peak remains. For the $Co/MoS_{2-x}$ (ED = 60 s) sample, after the acid etching step, the surface particles are gone (Figure 3g) and the two Co 2p peaks become weaker. This shows that the CoO particles are not stable during the acidic testing conditions of HER. Nevertheless, for both samples after acid etching, the remaining Co 2p XPS spectra are similar to those of atomic cobalt doped on $MoS_{2-x}$[25] and Co ion promoted amorphous $MoS_3$.[19] It is challenging for direct TEM observation of the Co−Mo bond for $Co/MoS_{2-x}$ on FTO (after acid etching) because of the small concentration of the Co atoms, the multilayer nature of the $MoS_2$ ,and the rough surface of FTO glass. To better understand the adsorption configuration of Co doping in $MoS_{2-x}$ (before etching), we performed Co K-edge XAS experiments. The Co K-edge XAS results (Figure 3m) show that the spectral shape of $Co/MoS_{2-x}$/FTO (ED = 60 s, before acid etching) is largely different from Co metal foil and $CoS_2$, which suggests the absence of Co−S bonds. This suggests that Co atoms are mainly presented in the forms of CoO[27] and Co−Mo before the etching process. Because acid etching removed CoO, the Co atom is in the form of Co−Mo in $Co/MoS_{2-x}$ on FTO (after acid etching), which is consistent with our DFT calculation configurations (Figure 2). The existence of the Co−Mo bond is more evident for samples supported on carbon foams (Figure 5d−g) because of larger X-ray absorption near-edge structure (XANES) and extended X-ray absorption fine structure (EXAFS) signals.

*HER Activity of $Co/MoS_{2-x}$ on FTO*. Figure 4a shows the polarization curves of pristine $MoS_2$, desulfurized $MoS_{2-x}$, $Co/MoS_2$, $Co/MoS_{2-x}$ (ED = 1 s), and Co directly deposited on FTO measured in 0.5 M $H_2SO_4$ electrolyte. These polarization curves were measured through linear sweep voltammetry with a scan rate of 10 mV/s, and they were *iR*-corrected. The current density values are calculated based on the projected area of the FTO substrate. The current density increases in the order of Co/FTO < $MoS_2$ < $MoS_{2-x}$ ≈ $Co/MoS_2$ < $Co/MoS_{2-x}$. The corresponding Tafel plots are shown in Figure 4b. The extracted Tafel slopes decrease as follows: Co/FTO of 189 mV/dec, $MoS_2$ of 125 mV/dec, $MoS_{2-x}$ of 118 mV/dec, $Co/MoS_2$ of 115 mV/dec, and $Co/MoS_{2-x}$ of 114 mV/dec. Though the Tafel slope of $Co/MoS_{2-x}$ is slightly greater than that of $Co/MoS_2$, its exchange current density ($9.206 \times 10^{-6}$ A/cm²) listed in Table S1 is about twice that of $Co/MoS_2$ ($5.205 \times 10^{-6}$ A/cm²), indicating the superior intrinsic catalytic activity of $Co/MoS_{2-x}$ over $Co/MoS_2$.[28] These results show that the HER activity of $MoS_2$ is increased after desulfurization, which is consistent with previous studies.[16] Notably, the HER activities of both $MoS_2$ and $MoS_{2-x}$ are improved after Co electrodeposition and the HER activity of $Co/MoS_{2-x}$ is higher than that of $Co/MoS_2$. It should be noted that when Co is directly deposited on FTO (Figure 4a, Co/FTO), it shows negligible activity for HER. These results are in an agreement with our DFT calculation that the HER activity is enhanced because of the synergy effect between Co atoms and the basal plane vacancies of $MoS_2$ support (Figure 2c).

We further measured the electrochemically active surface area (ECSA) using cyclic voltamograms (Figure S10) to further identify the origin of the higher HER activity of $Co/MoS_{2-x}$ over other samples. Figure 4c displays the normalized ECSA (black bars), current density at −0.3 V vs RHE (red bars), and current density per ECSA (blue bars) for several

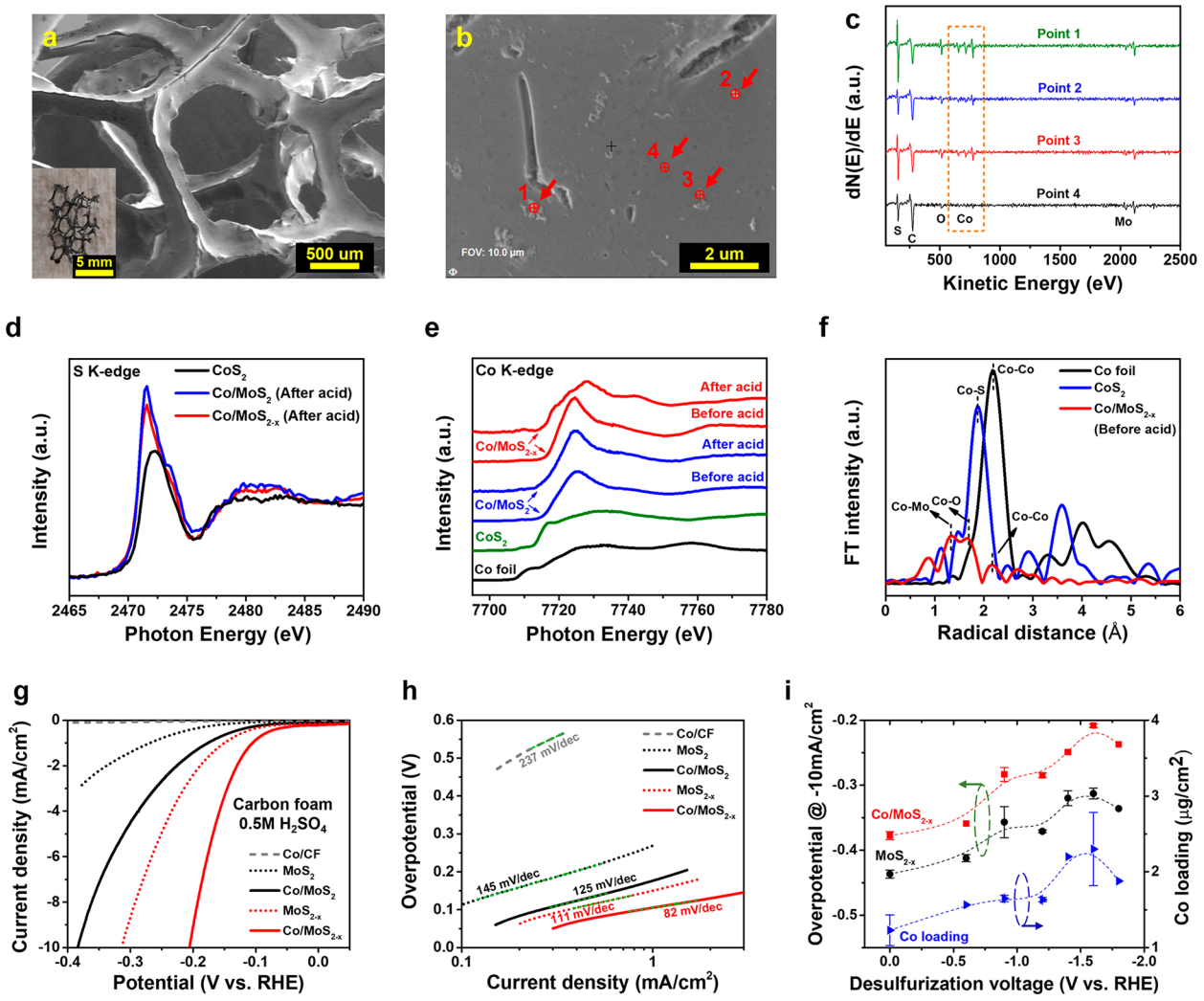


**Figure 5. Material and HER catalytic activity characterization of $Co/MoS_{2-x}$ film supported on carbon foams. (a and b) SEM images of low- and high-resolution for $Co/MoS_{2-x}$ (ED = 60 s, before acid etching) on carbon foam. The inset in panel a shows an optical image. (c) Differentiated AES spectra of the four different points marked in panel b. Points 1−3 show signals of Co. (d) S K-edge XANES spectra of $CoS_2$, $Co/MoS_2$, and $Co/MoS_{2-x}$ (ED = 60 s, after acid etching). (e) Co K-edge XANES spectra of Co metal foil, $CoS_2$, $Co/MoS_2$, and $Co/MoS_{2-x}$ (ED = 60 s, before and after acid etching). (f) Co K-edge EXAFS spectra of Co metal foil, $CoS_2$, and $Co/MoS_{2-x}$ (ED = 60 s, before acid etching). (g) Polarization curves of Co, $MoS_2$, $MoS_{2-x}$, $Co/MoS_2$ (ED = 1 s), and $Co/MoS_{2-x}$ (ED = 1 s) supported on carbon foam. (h) Corresponding Tafel plots of the cathodic sweeps of the polarization curves in panel g. (i) Overpotential of $Co/MoS_{2-x}$ (red, ED = 1 s) and $MoS_{2-x}$ (black) at −10 $mA/cm^2$ and the corresponding Co loading (blue) as a function of desulfurization voltage (ED = 1 s).**

samples, which are normalized by the pristine $MoS_2$ sample for comparison. The change in current density value reflects the combined change of ECSA (Figure 4c, black bars) and the intrinsic activity of each site. The ECSAs in $Co/MoS_2$ and $MoS_2$ are very similar. Therefore, the current density enhancement in $Co/MoS_2$ comes from the increase of intrinsic activity per active site. This is reasonable as Co is known to increase the intrinsic activity of S edge sites.[21,29] When $MoS_{2-x}$ is compared with $MoS_2$, the ECSA shows an apparent increase (1.7 times), which confirms newly created active sites of S-vacancies in the basal plane. The increase of current density is similar to that of ECSA here between $MoS_{2-x}$ and $MoS_2$, which shows that the basal plane S-vacancy has comparable activity with the S edge sites. Finally, the ECSA of $Co/MoS_{2-x}$ is even higher than $MoS_{2-x}$, indicating that Co addition leads to more active sites on the basal planes. The possible explanation is that some S-vacancies for $MoS_{2-x}$ are not in the optimal concentration range locally, so they do not contribute much to HER. After Co deposition, their HER activities are higher and become effective active sites. In addition, the enhanced intrinsic HER activity per site of $Co/MoS_{2-x}$ was estimated by dividing the normalized current density with the ECSA (Figure 4c, blue bar > 1), confirming our DFT calculation (Figure 2) in that the intrinsic active site density of S-vacancy is also improved with Co deposition.

We further tested the effect of Co deposition amount in $Co/MoS_{2-x}$ on HER activity. The Co amount (Figure 4d, black circles) is changed by varying the electrodeposition time from 0 to 10 s. Figure 4d shows the HER overpotential (defined as the potential to achieve −1 $mA/cm^2$) as a function of the Co electrodeposition time. The Co amount is estimated by integrating the deposition current−time curve with the assumption of all charges going to form Co (Figure S11b). The Co amount in $Co/MoS_{2-x}$ increases linearly with increasing the deposition time (Figure 4d). However, the overpotential decreases initially with increasing the deposition

time but saturates at around −0.23 V vs RHE after 250 ms of Co electrodeposition (Figure 4d). Considering the SEM and XPS results in Figure 3, a possible explanation is that the initial deposited Co atoms form chemical bonds with Mo atoms. As more Co atoms are deposited, they grow into CoO nanoparticles, as we observed from HRTEM of Co/$MoS_{2-x}$ (ED = 60 s, Figure 3i). Those CoO nanoparticles are dissolved during the HER test in acidic conditions. Co atoms that form chemical bonds with Mo atoms in the vacancy contribute to the HER activity. Finally, we did not vary the amount of Co deposition by varying the desulfurization voltage to change the S-vacancy concentration for $MoS_{2-x}$ on FTO because the higher desulfurization voltage deteriorates the adhesion between $MoS_2$ and FTO electrode. Such control study was carried out on carbon foams, as discussed in Figure 5f, because carbon foams have much better adhesion with $MoS_2$ than FTO.[16]

*HER Activity of Co/$MoS_{2-x}$ on Carbon Foams*. We further test if our Co deposition method will enhance $MoS_{2-x}$ deposited on three-dimensional substrates of more practical relevance. We changed the underneath substrate from flat FTO to commercial carbon foams (ERG Materials and Aerospace Corporation). The 2H phase polycrystalline $MoS_2$ multilayers were synthesized with the same thermolysis method as described in the Supporting Information. The SEM images of Co/$MoS_{2-x}$ (ED = 60 s) on the carbon foam are shown in Figure 5a, and the inset shows its optical image. The carbon foam has ∼10 pores per inch, and the pore diameter is about 2∼3 mm. The specific surface area of the carbon foam was determined by the Brunauer−Emmett−Teller (BET) method with xenon gas adsorption to be 132.32 $cm^2/g$. The presence of Co is confirmed by inspecting four points in Figure 5b by SEM/Auger electron spectroscopy (SEM/AES), where points 1−3 are selected on top of deposited particles and point 4 is not. The differentiated AES spectra in Figure 5c indicate that Co exists at points 1−3 with the kinetic energy of 658, 718, and 777 eV for Co and that point 4 is mainly $MoS_{2-x}$ without Co.

To better understand the adsorption configuration of S-vacancy and Co on Co/$MoS_{2-x}$ on carbon foam, we performed S and Co K-edge XAS experiments. The S K-edge peak intensity of Co/$MoS_{2-x}$ is weaker than that of Co/$MoS_2$ (Figure 5d), suggesting the formation of S-vacancy by the electrochemical desulfurization process.[30] The S K-edge at 2470 eV with the shoulder at 2473 eV indicates the Mo−S bond in $MoS_2$.[31] In addition, the S K-edge XANES results show that the spectral shapes of Co/$MoS_2$ and Co/$MoS_{2-x}$ are different from that of $CoS_2$, indicating the absence of Co−S bonds. The Co K-edge XANES results (Figure 5e) further show that both Co/$MoS_2$ and Co/$MoS_{2-x}$ before and after acid etching have different features with $CoS_2$ and Co metal foils. This suggests that Co atoms are mainly presented in the forms of Co−Mo and CoO before acid etching, consistent with the results for FTO substrates (Figure 3m). The Co XAS spectral shape changes significantly after acid etching with the main absorption edge shifting to lower energies (Figure 5e), which indicates that CoO is partially removed during the etching process. To further validate the results, we measured the Co K-edge EXAFS for Co/$MoS_{2-x}$ before acid etching. Co K-edge EXAFS is utilized to acquire structural parameters such as coordination numbers and bond lengths around Co. Figure 5f shows the Fourier transformed (FT) curves of Co/$MoS_{2-x}$ in comparison with the reference samples of $CoS_2$ and Co foil, and the corresponding $k^3$-weighted EXAFS $\chi(k)$ spectra are shown in Figure S12. The results show that no Co−S bonding configuration is observed; instead, the features at 1.8, 1.4, and 2.2 Å correspond to the Co−O, Co−Mo. and Co−Co[32,33] bonds, respectively. Because CoO is removed by the acid etching process, the remaining Co atoms are mainly bonded with Mo in $MoS_{2-x}$ with a lower oxidation state. In contrast, no apparent spectral shape change is observed for Co/$MoS_2$ before and after etching, suggesting that the bonding environment of Co atoms in $MoS_2$ after etching is different from that of $MoS_{2-x}$ after etching because of the presence of S-vacancies on $MoS_{2-x}$. Finally, we have also conducted similar EXAFS measurements for Co/$MoS_{2-x}$ on FTO, but the EXAFS signal is too weak to extract accurate information. The weak signal is due to the low loading amount of Co on a flat FTO substrate. The Co loading on porous carbon foam structure is much higher. Nevertheless, because we are preparing Co/$MoS_{2-x}$ on FTO and carbon foam using the same method and both substrates are inert, we expect that the EXAFS results on carbon foam should be applicable to FTO substrate as well.

Figure 5g shows the polarization curves of pristine $MoS_2$, desulfurized $MoS_{2-x}$, Co/$MoS_2$, Co/$MoS_{2-x}$ (ED = 1 s), and Co directly deposited on carbon foam (CF) measured in 0.5 M $H_2SO_4$ electrolyte. Similar with the results on FTO substrates (Figure 4a,b), the current density increases in the order of Co/CF < $MoS_2$ < Co/$MoS_2$ < $MoS_{2-x}$ < Co/$MoS_{2-x}$ (Figure 5g). The corresponding Tafel slopes (Figure 5h) and the exchange current density (Table S1) follow the trend of HER activity improvement. The overpotential for Co/$MoS_{2-x}$ on carbon foam is −0.21 V vs RHE (at 10 $mA/cm^2$), which is comparable to the state-of-the-art highly nanostructured $MoS_2$ catalyst (−0.25 to −0.11 V vs RHE).[4] The stability of Co/$MoS_{2-x}$ was tested using cyclic voltammograms for 1000 cycles between −0.3 and 0.2 V vs RHE at 100 mV/s. The *iR*-corrected initial and the final cathodic sweeps are shown in Figure S13. The overpotential at −10 $mA/cm^2$ decreased about 60 mV after the stability test. The instability is partially caused by hydrogen bubble generation, which exfoliates catalyst from the carbon foam. Another possible factor is the dissolution of a small amount of CoO nanoparticles. The stability is comparable to that of desulfurized $MoS_{2-x}$ and better than that of amorphous cobalt sulfide ($CoS_x$) whose overpotential at −5 $mA/cm^2$ degrades about 250 mV after 500 potential sweeps.[20]

Finally, we also tested the effect of Co loading on the HER activity of Co/$MoS_{2-x}$/CF (ED = 1 s) by varying the desulfurization voltage. The desulfurization was carried out under each voltage for 3 min using chronoamperometry in 0.5 M $H_2SO_4$ electrolyte solution, the same as our previous work.[16] Figure 5i plots the HER overpotential (left *y*-axis), defined as the potential to achieve −10 $mA/cm^2$, for $MoS_{2-x}$ (black) and Co/$MoS_{2-x}$ (red) and the total Co loading (right *y*-axis) as a function of the desulfurization voltage. As the desulfurization voltage increases, higher concentration of S-vacancy is generated, which leads to first reduced and then increased overpotential for $MoS_{2-x}$. This is consistent with previous DFT results in that there is an optimal range S-vacancy for the HER activity.[13] Similarly, more S-vacancy provides more nucleation sites for Co, leading to higher loading of Co and lower overpotential for Co/$MoS_{2-x}$. These results show that the HER activity of $MoS_2$ can be improved by the combination of S-vacancy and Co deposition.

In summary, our combined DFT calculations and experiments have demonstrated that embedded Co atoms can significantly enhance the HER activity of both pristine $MoS_2$ and desulfurized $MoS_{2-x}$ multilayers. According to our DFT calculations, there is a desirable synergy effect between the Co atoms directly connected to the S-vacancies, which provide a favorable site for hydrogen adsorption. Our experimental results show, for the control $Co/MoS_2$ sample, the Co atoms are mainly incorporated into the edge sites and their addition has little impact on ECSA but enhances the activity per unit site, as expected. In contrast, for $Co/MoS_{2-x}$, the Co atoms are incorporated into both basal planes and edge sites. Importantly, the embedded Co increases both ECSA and the activity per active site, suggesting an improvement of the activity of basal plane S-vacancies. For the desulfurized $MoS_{2-x}$ multilayers supported on carbon foams, the deposition of Co reduces the overpotential at $-10$ mA/cm$^2$ from $-0.32$ to $-0.21$ V vs RHE for $Co/MoS_{2-x}$, which is comparable to the state-of-the-art $MoS_2$-based catalysts ($-0.25$ to $-0.11$ V vs RHE). The results of this work demonstrate the effect and potential of modifying the intrinsic basal plane S-vacancy activity with transition-metal atoms, which could be applied to other catalytic reactions as well.

## ■ ASSOCIATED CONTENT

### Supporting Information

The Supporting Information is available free of charge on the ACS Publications website at DOI: 10.1021/acsenergylett.8b01567.

Experimental and Computational Methods; DFT models; Raman spectra, XPS, TEM, HAADF-STEM, EDS, exchange current density, capacitive current, electrodeposition, EXAFS $\chi$(k) spectra, and stability results (PDF)

## ■ AUTHOR INFORMATION


### Corresponding Authors

*E-mail: samiras@stanford.edu.
*E-mail: xlzheng@stanford.edu.

### ORCID

Sangwook Park: 0000-0003-0939-1696
Hadi Abroshan: 0000-0003-1046-5170
Liang Zhang: 0000-0002-3446-3172
Jung Kyu Kim: 0000-0002-8218-0062
Jinghua Guo: 0000-0002-8576-2172
Samira Siahrostami: 0000-0002-1192-4634
Xiaolin Zheng: 0000-0002-8889-7873


### Author Contributions

$^{\nabla}$S.P., J.P., and H.A. contributed equally to this work. S.P., J.P., J.K.K., and X.Z. conceived the idea and designed the experiments. S.P. performed the material growth, electrode fabrication, material characterization, and electrochemical measurements. J.P. and J.Z. conducted the SEM, TEM, HAADF-STEM, and EDS characterizations. J.K.K. designed the schematic of the experimental process. S.S. conceived and designed the DFT calculations. H.A. performed the DFT calculations. L.Z. and J.G. conducted XAS experiments and analysis. S.P., J.P., X.Z., S.S., and H.A. wrote the manuscript, and all authors discussed the results and commented on the manuscript.

### Notes

The authors declare no competing financial interest.

## ■ ACKNOWLEDGMENTS


X.Z. acknowledges generous financial support from Stanford Natural Gas Initiative (NGI), Stanford Precourt Institute of Energy (PIE), and Samsung Global Research Outreach (GRO) Program under the supervision of Dr. Un Jeong Kim. Part of this work (XPS, SEM, FIB, and TEM data) was performed at Stanford Nano Shared Facilities (SNSF) and Hewlett-Packard Lab. The work at Advanced Light Source of the Lawrence Berkeley National Laboratory was supported by the Director, Office of Science, Office of Basic Energy Sciences, of the U.S. Department of Energy under Contract No. DE-AC02-05CH11231. We thank beamline scientist Sirine Fakra for her strong technical support.


## ■ REFERENCES


(1) Dresselhaus, M. S.; Thomas, I. L. Alternative Energy Technologies. *Nature* **2001**, *414*, 332−337.

(2) Hinnemann, B.; Moses, P. G.; Bonde, J.; Jorgensen, K. P.; Nielsen, J. H.; Horch, S.; Chorkendorff, I.; Norskov, J. K. Biomimetic Hydrogen Evolution $MoS_2$ Nanoparticles as Catalyst for Hydrogen Evolution. *J. Am. Chem. Soc.* **2005**, *127*, 5308−5309.

(3) Merki, D.; Hu, X. Recent Developments of Molybdenum and Tungsten Sulfides as Hydrogen Evolution Catalysts. *Energy Environ. Sci.* **2011**, *4*, 3878−3888.

(4) Benck, J. D.; Hellstern, T. R.; Kibsgaard, J.; Chakthranont, P.; Jaramillo, T. F. Catalyzing the Hydrogen Evolution Reaction (HER) with Molybdenum Sulfide Nanomaterials. *ACS Catal.* **2014**, *4*, 3957−3971.

(5) Yin, Y.; Han, J.; Zhang, Y.; Zhang, X.; Xu, P.; Yuan, Q.; Samad, L.; Wang, X.; Wang, Y.; Zhang, Z.; et al. Contributions of Phase, Sulfur Vacancies, and Edges to the Hydrogen Evolution Reaction Catalytic Activity of Porous Molybdenum Disulfide Nanosheets. *J. Am. Chem. Soc.* **2016**, *138*, 7965−7972.

(6) Ding, Q.; Song, B.; Xu, P.; Jin, S. Efficient Electrocatalytic and Photoelectrochemical Hydrogen Generation Using $MoS_2$ and Related Compounds. *Chem.* **2016**, *1*, 699−726.

(7) Jaramillo, T. F.; Jorgensen, K. P.; Bonde, J.; Nielsen, J. H.; Horch, S.; Chorkendorff, I. Identification of Active Edge Sites for Electrochemical $H_2$ Evolution from $MoS_2$ Nanocatalysts. *Science* **2007**, *317*, 100−102.

(8) Kibsgaard, J.; Chen, Z.; Reinecke, B. N.; Jaramillo, T. F. Engineering the Surface Structure of $MoS_2$ to Preferentially Expose Active Edge Sites for Electrocatalysis. *Nat. Mater.* **2012**, *11*, 963−969.

(9) Tsai, C.; Chan, K.; Nørskov, J. K.; Abild-Pedersen, F. Theoretical Insights into the Hydrogen Evolution Activity of Layered Transition Metal Dichalcogenides. *Surf. Sci.* **2015**, *640*, 133−140.

(10) Kong, D.; Wang, H.; Cha, J. J.; Pasta, M.; Koski, K. J.; Yao, J.; Cui, Y. Synthesis of $MoS_2$ and $MoSe_2$ Films with Vertically Aligned Layers. *Nano Lett.* **2013**, *13*, 1341−1347.

(11) Sun, Y.; Alimohammadi, F.; Zhang, D.; Guo, G. Enabling Colloidal Synthesis of Edge-Oriented $MoS_2$ with Expanded Interlayer Spacing for Enhanced HER Catalysis. *Nano Lett.* **2017**, *17*, 1963−1969.

(12) Kiriya, D.; Lobaccaro, P.; Nyein, H. Y.; Taheri, P.; Hettick, M.; Shiraki, H.; Sutter-Fella, C. M.; Zhao, P.; Gao, W.; Maboudian, R.; et al. General Thermal Texturization Process of $MoS_2$ for Efficient Electrocatalytic Hydrogen Evolution Reaction. *Nano Lett.* **2016**, *16*, 4047−4053.

(13) Li, H.; Tsai, C.; Koh, A. L.; Cai, L.; Contryman, A. W.; Fragapane, A. H.; Zhao, J.; Han, H. S.; Manoharan, H. C.; Abild-Pedersen, F.; et al. Activating and Optimizing $MoS_2$ Basal Planes for Hydrogen Evolution through the Formation of Strained Sulphur Vacancies. *Nat. Mater.* **2016**, *15*, 48−53.

(14) Li, H.; Du, M.; Mleczko, M. J.; Koh, A. L.; Nishi, Y.; Pop, E.; Bard, A. J.; Zheng, X. Kinetic Study of Hydrogen Evolution Reaction over Strained $MoS_2$ with Sulfur Vacancies Using Scanning Electrochemical Microscopy. *J. Am. Chem. Soc.* **2016**, *138*, 5123−5129.
(15) Ye, G.; Gong, Y.; Lin, J.; Li, B.; He, Y.; Pantelides, S. T.; Zhou, W.; Vajtai, R.; Ajayan, P. M. Defects Engineered Monolayer $MoS_2$ for Improved Hydrogen Evolution Reaction. *Nano Lett.* **2016**, *16*, 1097−1103.
(16) Tsai, C.; Li, H.; Park, S.; Park, J.; Han, H. S.; Norskov, J. K.; Zheng, X.; Abild-Pedersen, F. Electrochemical Generation of Sulfur Vacancies in the Basal Plane of $MoS_2$ for Hydrogen Evolution. *Nat. Commun.* **2017**, *8*, 15113.
(17) Xia, B.; Wang, T.; Jiang, X.; Zhang, T.; Li, J.; Xiao, W.; Xi, P.; Gao, D.; Xue, D.; Ding, J. $Ar^{2+}$ Beam Irradiation-Induced Multivancancies in $MoSe_2$ Nanosheet for Enhanced Electrochemical Hydrogen Evolution. *ACS Energy Lett.* **2018**, *3*, 2167−2172.
(18) Gao, D.; Xia, B.; Wang, Y.; Xiao, W.; Xi, P.; Xue, D.; Ding, J. Dual-Native Vacancy Activated Basal Plane and Conductivity of $MoSe_2$ with High-Efficiency Hydrogen Evolution Reaction. *Small* **2018**, *14*, 1704150.
(19) Merki, D.; Vrubel, H.; Rovelli, L.; Fierro, S.; Hu, X. Fe, Co, and Ni Ions Promote the Catalytic Activity of Amorphous Molybdenum Sulfide Films for Hydrogen Evolution. *Chem. Sci.* **2012**, *3*, 2515−2525.
(20) Staszak-Jirkovsky, J.; Malliakas, C. D.; Lopes, P. P.; Danilovic, N.; Kota, S. S.; Chang, K. C.; Genorio, B.; Strmcnik, D.; Stamenkovic, V. R.; Kanatzidis, M. G.; et al. Design of Active and Stable Co-Mo-$S_x$ Chalcogels as pH-Universal Catalysts for the Hydrogen Evolution Reaction. *Nat. Mater.* **2016**, *15*, 197−203.
(21) Wang, H.; Tsai, C.; Kong, D.; Chan, K.; Abild-Pedersen, F.; Nørskov, J. K.; Cui, Y. Transition-Metal Doped Edge Sites in Vertically Aligned $MoS_2$ Catalysts for Enhanced Hydrogen Evolution. *Nano Res.* **2015**, *8*, 566−575.
(22) Chen, Y.-Y.; Dong, M.; Wang, J.; Jiao, H. Mechanisms and Energies of Water Gas Shift Reaction on Fe-, Co-, and Ni-Promoted $MoS_2$ Catalysts. *J. Phys. Chem. C* **2012**, *116*, 25368−25375.
(23) Zhang, C.; Liu, B.; Zhao, L.; Zong, Q.; Gao, J.; Wang, Y.; Xu, C. Insights into Water−Gas Shift Reaction Mechanisms over $MoS_2$ and Co-$MoS_2$ Catalysts: A Density Functional Study. *React. Kinet., Mech. Catal.* **2017**, *120*, 833−844.
(24) Xiao, B. B.; Zhang, P.; Han, L. P.; Wen, Z. Functional $MoS_2$ by the Co/Ni Doping as the Catalyst for Oxygen Reduction Reaction. *Appl. Surf. Sci.* **2015**, *354*, 221−228.
(25) Liu, G.; Robertson, A. W.; Li, M. M.; Kuo, W. C. H.; Darby, M. T.; Muhieddine, M. H.; Lin, Y. C.; Suenaga, K.; Stamatakis, M.; Warner, J. H.; et al. $MoS_2$ Monolayer Catalyst Doped with Isolated Co Atoms for the Hydrodeoxygenation Reaction. *Nat. Chem.* **2017**, *9*, 810−816.
(26) Liu, K. K.; Zhang, W.; Lee, Y. H.; Lin, Y. C.; Chang, M. T.; Su, C. Y.; Chang, C. S.; Li, H.; Shi, Y.; Zhang, H.; et al. Growth of Large-Area and Highly Crystalline $MoS_2$ Thin Layers on Insulating Substrates. *Nano Lett.* **2012**, *12*, 1538−1544.
(27) Chen, L.; Mashimo, T.; Iwamoto, C.; Okudera, H.; Omurzak, E.; Ganapathy, H. S.; Ihara, H.; Zhang, J.; Abdullaeva, Z.; Takebe, S.; et al. Synthesis of Novel $CoC_x$@C Nanoparticles. *Nanotechnology* **2013**, *24*, 045602.
(28) Seo, B.; Joo, S. H. Recent Advances in Unveiling Active Sites in Molybdenum Sulfide-Based Electrocatalysts for the Hydrogen Evolution Reaction. *Nano Convergence* **2017**, *4*, 19.
(29) Dai, X.; Du, K.; Li, Z.; Liu, M.; Ma, Y.; Sun, H.; Zhang, X.; Yang, Y. Co-Doped $MoS_2$ Nanosheets with the Dominant CoMoS Phase Coated on Carbon as an Excellent Electrocatalyst for Hydrogen Evolution. *ACS Appl. Mater. Interfaces* **2015**, *7*, 27242−27253.
(30) Huber, S. P.; Gullikson, E.; Meyer-Ilse, J.; Frye, C. D.; Edgar, J. H.; van de Kruijs, R. W. E.; Bijkerk, F.; Prendergast, D. Detection of Defect Populations in Superhard Semiconductor Boron Subphosphide $B_{12}P_2$ through X-ray Absorption Spectroscopy. *J. Mater. Chem. A* **2017**, *5*, 5737−5749.
(31) Cesano, F.; Bertarione, S.; Piovano, A.; Agostini, G.; Rahman, M. M.; Groppo, E.; Bonino, F.; Scarano, D.; Lamberti, C.; Bordiga, S.; et al. Model Oxide Supported $MoS_2$ HDS Catalysts: Structure and Surface Properties. *Catal. Sci. Technol.* **2011**, *1*, 123−136.
(32) Sun, Z.; Yan, W.; Yao, T.; Liu, Q.; Xie, Y.; Wei, S. XAFS in Dilute Magnetic Semiconductors. *Dalton trans.* **2013**, *42*, 13779−13801.
(33) Park, J.-W.; Park, C.-M. Mechanochemically Induced Transformation of CoO(OH) into $Co_3O_4$ Nanoparticles and Their Highly Reversible Li Storage Characteristics. *RSC Adv.* **2017**, *7*, 10618−10623.